The spectrum of singlet SiH_2[1]

S.N. Yurchenko, P.R. Bunker, W.P. Kraemer, and P. Jensen

Abstract: We report a theoretical study of the two lowest singlet electronic states ($\tilde{X}\,^1A_1$ and $\tilde{A}\,^1B_1$) of silylene SiH_2. These states become degenerate as a $^1\Delta_g$ state at linear configurations and are subject to the Renner effect. In ab initio calculations we have determined the potential energy and dipole moment surfaces for each state, and the transition moment surface between the states. Parameterized analytical functions have been fitted through the various sets of ab initio points, and the parameter values obtained for the potential energy surfaces have been further refined in fittings to experimental spectroscopic data. In these latter fittings, we use as input data experimentally derived energy differences together with ab initio points. In this manner, we achieve refined potential energy surfaces that behave reasonably also in regions of configuration space that are not sampled by the wavefunctions of the states for which experimentally derived energies are available. The calculation of rovibronic energies, the fittings to experimentally derived energies, and simulations of $\tilde{A}\,^1B_1 \rightarrow \tilde{X}\,^1A_1$ emission spectra of SiH_2 have been carried out with the RENNER program system. The higher excited vibrational states of $\tilde{X}\,^1A_1$ SiH_2 form polyads of heavily interacting states and many polyad states have been observed in dispersed fluorescence studies. The present theoretical work shows that owing to the heavy interaction between the states in the polyads, it is difficult to obtain unambiguous assignments for them.

Key words: silylene, RENNER, ab initio.

PACS Nos.: 31.15.Ar, 33.20.Wr, 33.20.Ea

Résumé : On a effectué une étude théorique des deux états électroniques singulets les plus faibles, $\tilde{X}\,^1A_1$ et $\tilde{A}\,^1B_1$ du silylène, SiH_2. Ces états deviennent dégénérés sous la forme d'un état $^1\Delta_g$ à configurations linéaires et ils sont sujets à l'effet de Renner. Dans les calculs ab initio, il a été possible de déterminer pour chaque état les surfaces de l'énergie potentielle et du moment dipolaire et la surface du moment de transition entre les états. Faisant appel à divers ensembles de points ab initio, on a ajusté des fonctions analytiques paramétrisées et on a mieux affiné les valeurs des paramètres obtenus pour les surfaces d'énergie potentielle en les ajustant aux données spectroscopiques expérimentales. Dans ces derniers ajustements, on a utilisé les données de base les différences d'énergie obtenues expérimentalement ainsi que les points *ab initio*. De cette façon, on a réussi à affiner les surfaces d'énergie potentielle de façon à ce qu'elles se comportent raisonnablement aussi dans des régions de l'espace de configuration qui ne sont pas soumises à l'échantillonnage des fonctions d'onde des états et pour lesquelles des énergies obtenues à partir de données expérimentales sont disponibles. Le calcul des énergies rovibroniques, les ajustements aux énergies obtenues à partir de données expérimentales et les simulations des spectres d'émission $\tilde{A}\,^1B_1 \rightarrow \tilde{X}\,^1A_1$ du SiH_2 ont été réalisés à l'aide du système de programme RENNER. L'état vibrationnel excité le plus élevé ($\tilde{X}\,^1A_1$) du SiH_2 forme des polyads d'états interagissant fortement et on a observé plusieurs états polyads dans le cadre d'études de fluorescence dispersée. Le présent travail théorique montre qu'en raison des fortes interactions entre les états des polyads, il est difficile d'obtenir des attributions non ambiguës pour eux.

Mots clés : silylène, RENNER, ab initio.

[Traduit par la Rédaction]

1. Introduction

Thin silicon films are essential for the industrial production of solar cells and semiconductor devices, and such films are produced by chemical vapour deposition following the decomposition of silane SiH_4. Silylene SiH_2 is a significant intermediate formed during decomposition reactions of SiH_4, and this paper is a contribution to the theoretical analysis of its spectra.

In contrast to the situation for methylene, the ground state of silylene is a singlet state: $\tilde{X}\,^1A_1$. The first excited state is the $\tilde{a}\,^3B_1$ state, and above that is the first excited singlet state $\tilde{A}\,^1B_1$. All these states are bent at equilibrium. At linearity the two singlet states become degenerate forming a $^1\Delta_g$ electronic state. As a result of this degeneracy at linearity there is a Renner effect interaction between the rovibronic levels of the $\tilde{X}$ and $\tilde{A}$

Received 2 October 2003. Published on the NRC Research Press Web site at http://canjchem.nrc.ca/ on 15 June 2004.

S.N. Yurchenko[2,3] and P.R. Bunker. Steacie Institute for Molecular Sciences, National Research Council of Canada, Ottawa ON K1A 0R6, Canada.
W.P. Kraemer. Max Planck Institute of Astrophysics, Karl-Schwarzschild-Strasse 1, Postfach 1523, D-85740 Garching, Germany.
P. Jensen. FB 9 - Theoretische Chemie, Bergische Universität, D-42097 Wuppertal, Germany.

[1]This article is part of a Special Issue dedicated to the memory of Professor Gerhard Herzberg.
[2]Present Address: Max-Planck-Institut für Kohlenforschung, Kaiser-Wilheim-Platz 1, D-45470 Mülheim an der Rurh, Germany.
[3]Corresponding author (e-mail: yurchenk@uni-wuppertal.de).

 doi: 10.1139/V04-030

electronic states. The theory of the Renner effect is reviewed, for example, in refs. 1 and 2. We report here a theoretical study of the spectra associated with the $\tilde{X}$ and $\tilde{A}$ singlet states of silylene.

The first observation of SiH_2 was made by Dubois et al. (3) who recorded the $\tilde{A}\,^1B_1 \leftarrow \tilde{X}\,^1A_1$ absorption spectrum in the visible region. Dubois and co-workers (4,5) subsequently rotationally analyzed the progression of bands $\tilde{A}\,^1B_1\ (0, v_2, 0) \leftarrow \tilde{X}\,^1A_1\ (0, 0, 0)$ with $v_2 = 1-6$ and Francisco et al. (6) obtained the vibrational energies of the $\tilde{A}\,^1B_1$ (0,7,0) and $\tilde{A}\,^1B_1$ (0,8,0) states. We use the notation $\tilde{X}\,^1A_1\ (v_1, v_2, v_3)$ or $\tilde{A}\,^1B_1\ (v_1, v_2, v_3)$ for the vibronic states, where v_2 is the vibrational quantum number appropriate for a bent molecule. Escribano and Campargue (7) observed and analyzed the $\tilde{A}\,^1B_1\ (0, 0, 0) \leftarrow \tilde{X}\,^1A_1\ (0, 0, 0)$ band in 1998 with significantly higher resolution than had been available in the earlier studies. Laser-induced fluorescence (LIF) studies of the $\tilde{A}$ state were reported by Ishikawa and Kajimoto (8). In 1989, Yamada et. al (9) used IR diode laser kinetic spectroscopy to observe the v_2 band of the $\tilde{X}$ state, and 2 years later Ishikawa and Kajimoto (10) obtained several $\tilde{X}$ state vibrational term values in a dispersed fluorescence experiment. This latter work was reanalyzed by Ishikawa and Kajimoto (11) and updated by Hirota and Ishikawa (12) in their analysis of the vibrational energy level structure of the $\tilde{X}$ state. LIF excitation and dispersed fluorescence studies of SiH_2 and SiD_2 were reported by Fukushima et al. (13) and Fukushima and Obi (14). Finally, in 2002 Ishikawa et al. (15) carried out an extensive stimulated emission pumping study of the $\tilde{A}$–$\tilde{X}$ system, obtaining a wealth of $\tilde{X}$-state vibrational term values (up to 9800 cm^{-1}above the $\tilde{X}$ vibrational ground state level) together with some information about the spin-orbit interaction between the $\tilde{X}\,^1A_1$ and the $\tilde{a}\,^3B_1$ electronic states.

On the theoretical side ab initio work involving limited dimensionality calculations of the potential energy surfaces have been performed, and the only full three-dimensional surfaces are those of the $\tilde{X}$ and $\tilde{a}$ states by Gabriel et. al (16) in a coupled-electron-pair-approach (CEPA) calculation (17). They calculated also rovibronic energies, spectroscopic constants, dipole moment parameters, and intensities. In 1993, Duxbury et. al (18) reanalyzed the available experimental data on $\tilde{X}$-state and $\tilde{A}$-state SiH_2 with a semiquantitative model incorporating the Renner interaction between the two states and the spin-orbit interaction with the $\tilde{a}\,^3B_1$ electronic state.

In the present study, we first made an ab initio calculation of the potential energy surfaces, and the dipole moment and transition moment surfaces, for the $\tilde{X}\,^1A_1$ and $\tilde{A}\,^1B_1$ states of SiH_2. Using the ab initio potential surfaces, we calculated rovibronic energies and compared them with experimental results. We then refined the potential energy surfaces in fittings to the large amount of experimentally derived rovibronic energy values available for the $\tilde{X}$ state of SiH_2, and to the energies available for the $\tilde{A}$ state. In these fittings, we used the ab initio information to constrain the potential energy surfaces so that they remained relatively close to the initial ab initio surfaces in regions of configuration space that are not sampled by the wavefunctions for the experimentally characterized states. We also present predictions for the energies of highly excited vibrational states calculated with the refined potential energy parameters, and we simulate the $\tilde{A}\,^1B_1 \rightarrow \tilde{X}\,^1A_1$ emission spectrum for comparison with the results of the stimulated emission pumping experiments of Ishikawa et al. (15). In some of these experiments, the molecules are pumped to the 0_{00} rotational level in either the $\tilde{A}(060)$ or $\tilde{A}(070)$ state, and the measured emission

Table 1. Potential energy parameters[a] for the $\tilde{X}\,^1A_1$ and $\tilde{A}\,^1B_1$ electronic states of SiH_2 (see eqs. [1]–[5] for the definitions of the parameters).

Parameter[b]	MCI ab initio[c]	Fitted
V_{ref}(hartree)	−290.075 28 (11)[d]	
$r_{12}^{(ref)}$ (Å)	1.489 089 13 (13)	1.489 089[e]
a_1 ($Å^{-1}$)	1.58[e]	1.58[e]
$f_{11}^{(0)}$	24 664 (207)	25 950 (22)
$f_{13}^{(0)}$	−372 (295)	−133 (22)
$f_{111}^{(0)}$	−2 592 (280)	−3 392 (77)
$f_{1111}^{(0)}$	1 293 (759)	2 941 (83)
$f_0^{(1,-)}$	−69 346 (387)	−68 962 (46)
$f_0^{(2,-)}$	103 276 (2034)	103 841 (81)
$f_0^{(3,-)}$	−106 731 (4539)	−108 072 (65)
$f_0^{(4,-)}$	73 767 (4951)	74 690 (12)
$f_0^{(5,-)}$	−27 365 (2601)	−27 783 (17)
$f_0^{(6,-)}$	4 406 (525)	4 549 (46)
$f_1^{(1,-)}$	−10 165 (183)	−10 095 (12)
$f_1^{(2,-)}$	17 448 (584)	17 340 (12)
$f_1^{(3,-)}$	−12 097 (599)	−12 320 (64)
$f_1^{(4,-)}$	2 333 (192)	2 585 (69)
$f_{11}^{(1,-)}$	4 265 (327)	2 650 (52)
$f_{11}^{(2,-)}$	−1 848 (204)	−1 662 (56)
$f_{111}^{(1,-)}$	10 836 (2129)	18 155 (115)
$f_{111}^{(2,-)}$	−7 878 (2062)	−13 534 (89)
$f_{113}^{(1,-)}$	−5 994 (1963)	−3 903 (219)
$f_0^{(1,+)}$	−44 077 (434)	−41 555 (58)
$f_0^{(2,+)}$	122 536 (3154)	112 569 (16)
$f_0^{(3,+)}$	−198 108 (9700)	−177 201 (18)
$f_0^{(4,+)}$	201 047 (14156)	177 276 (19)
$f_0^{(5,+)}$	−107 205 (9731)	−93 592 (24)
$f_0^{(6,+)}$	23 643 (2530)	20 587 (15)
$f_1^{(1,+)}$	4 818 (264)	3 663 (51)
$f_1^{(2,+)}$	−14 579 (1134)	−7 502 (148)
$f_1^{(3,+)}$	13 350 (1549)	1 524 (99)
$f_1^{(4,+)}$	−5 328 (669)	0
$f_{11}^{(1,+)}$	4 413 (452)	884 (98)
$f_{11}^{(3,+)}$	−4 873 (431)	−4 146 (127)
$f_{13}^{(2,+)}$	2 439 (969)	0

[a] Units are cm^{-1} unless otherwise indicated.
[b] Parameters for the $\tilde{X}$ state are denoted with a "−" in the superscript, and those for the $\tilde{A}$ state with a "+".
[c] After lowering the barrier to linearity by 150 cm^{-1} (see text).
[d] Quantities in parentheses are standard errors in units of the last digit quoted.
[e] Held fixed in the respective least-squares fittings.

Table 2. The ab initio dipole and transition moment parameters for the $\tilde{X}\,^1A_1$ and $\tilde{A}\,^1B_1$ electronic states of SiH_2 (see eqs. [9]–[13] for the definitions of the parameters).

$\widetilde{X}^1A_1$		$\widetilde{A}\,^1B_1$		$\widetilde{X}/\widetilde{A}$	
$q_0^{(0;-)}$ (D)	5.238(38)[a]	$q_0^{(0;+)}$ (D)	2.927(23)	$x_0^{(0;\pm)}$ (D)	−1.413(16)
$q_0^{(1;-)}$ (D)	−24.25(64)	$q_0^{(1;+)}$ (D)	−20.22(38)	$x_0^{(1;\pm)}$ (D)	0.548(50)
$q_0^{(2;-)}$ (D)	69.1(36)	$q_0^{(2;+)}$ (D)	64.4(21)	$x_0^{(5;\pm)}$ (D)	1.41(52)
$q_0^{(3;-)}$ (D)	−119.7(95)	$q_0^{(3;+)}$ (D)	−116.4(55)	$x_0^{(6;\pm)}$ (D)	−0.32(20)
$q_0^{(4;-)}$ (D)	117.4(123)	$q_0^{(4;+)}$ (D)	116.5(71)	$x_1^{(1;\pm)}$ (D Å^{-1})	0.906(23)
$q_0^{(5;-)}$ (D)	−60.1(77)	$q_0^{(5;+)}$ (D)	−60.4(45)	$x_{11}^{(0;\pm}$ (D Å^{-2})	0.123(78)
$q_0^{(6;-)}$ (D)	12.5(19)	$q_0^{(6;+)}$ (D)	12.6(11)	$x_{111}^{(0;\pm)}$ (D Å^{-3})	3.3(20)
$q_1^{(0;-)}$ (D Å^{-1})	−1.694(36)	$q_1^{(0;+)}$ (D Å^{-1})	−0.526(21)	$x_{113}^{(0;\pm)}$ (D Å^{-3})	−4.8(20)
$q_1^{(1;-)}$ (D Å^{-1})	0.123(31)	$q_1^{(1;+)}$ (D Å^{-1})	0.717(21)	Std. Dev.[b] (D)	0.023
$q_{11}^{(0;-)}$ (D Å^{-2})	−0.611(76)	$q_{13}^{(0;+)}$ (D Å^{-2})	−0.219(88)		
$q_{111}^{(0;-)}$ (D Å^{-3})	1.09(68)	$q_{111}^{(0;+)}$ (D Å^{-3})	−0.92(40)		
Std. Dev.[b](D)	0.076	Std. Dev.[b] (D)	0.012		
$p_1^{(0;-)}$ (D Å^{-1})	−0.240(46)	$p_1^{(0;+)}$ (D Å^{-1})	−0.253(25)		
$p_1^{(1;-)}$ (D Å^{-1})	12.35(61)	$p_1^{(1;+)}$ (D Å^{-1})	6.5(75)		
$p_1^{(2;-)}$ (D Å^{-1})	−27.0(21)	$p_1^{(2;+)}$ (D Å^{-1})	−16.4(29)		
$p_1^{(3;-)}$ (D Å^{-1})	24.0(25)	$p_1^{(3;+)}$ (D Å^{-1})	16.7(35)		
$p_1^{(4;-)}$ (D Å^{-1})	−7.39(93)	$p_1^{(4;+)}$ (D Å^{-1})	−5.6(14)		
$p_{111}^{(0;-)}$ (D Å^{-3})	4.5(16)	$p_{113}^{(0;+)}$ (D Å^{-3})	−4.3(26)		
$p_{113}^{(0;-)}$ (D Å^{-3})	−15.5(48)	$p_{1111}^{(0;+)}$ (D Å^{-4})	−5.2(26)		
		$p_{1111}^{(0;+)}$ (D Å^{-4})	11.2(99)		
Std. Dev.[b] (D)	0.0079	Std. Dev.[b] (D)	0.011		

[a]Quantities in parentheses are standard errors in units of the last digit quoted.
[b]Standard deviation of the fitting to the ab initio points.

spectra consist of the allowed $1_{10} \leftarrow 0_{00}$ rotational transition to vibrational levels of the $\tilde{X}$ state. In other experiments the $\tilde{A}(010)\ 1_{01}$ level is pumped and the spectra then consist of rotational transitions to both the 1_{11} and 2_{11} levels of vibrational levels of the $\tilde{X}$ state.

2. Ab initio calculations

Ab initio calculations of the potential energy surfaces were performed for the $\tilde{X}\,^1A_1$ and $\tilde{A}\,^1B_1$ singlet electronic states. The geometries involved a range of the HSiH bond angles (30°–160°) and SiH bond lengths (1.27–1.72 Å) including asymmetric bond stretches. The C_s point group symmetry was therefore used to classify the electronic wavefunctions.

General contraction type atomic natural orbital (ANO) bases were chosen to approximate the molecular orbitals. They consist for silicon of $17s$-, $12p$-, $5d$-, and $3f$-type functions contracted to $(7s6p4d3f)$-functions, and for the hydrogens of $8s$-, $4p$-, and $3d$-type functions contracted to $(6s4p3d)$-functions; in total 176 primitive functions contracted to 132 functions.

The energies were evaluated at the multireference configuration interaction (MR-CI) level of theory using molecular orbital bases that were optimized for each state separately by complete-active-space (CASSCF) calculations. The CASSCF partitioning scheme adopted here keeps the 10 electrons occupying the Si $1s$, $2s$, and $2p$ orbitals inactive and allows the remaining six valence electrons to be distributed among six active orbitals (4 a' orbitals and 2 a'' orbitals) in all possible ways consistent with the respective space and spin symmetries. In the MR-CI calculations these CASSCF wavefunctions (100 configuration state functions (CSFs) for the $\tilde{X}$ state and 80 CSFs for the $\tilde{A}$ state) are used as reference configurations from which all single and double excitations are generated. The total CI-expansions of the two states comprise 763 860 and 776 750 CSFs, respectively. The present calculations made use of the MOLCAS program system (19).

The equilibrium geometry parameters determined at this level of theory are close to the r_0 experimental parameters (4), and to those obtained recently in other high accuracy ab initio studies (16, 20, 21). For the strongly bent $\tilde{X}$ state the equilibrium bond angle is obtained as 92.4°, and the SiH bond length as $r_e = 1.5185$ Å. For the $\tilde{A}$ state, the equilibrium angle is 122.9° and the equilibrium bond length is found to be slightly shorter at $r_e = 1.4874$ Å. The equilibrium energy separation between the two singlet states is calculated as $T_e(\tilde{A}) = 15\,677\ cm^{-1}$, and from experiment (7) $T_0(\tilde{A}) = 15\ 547.773\ cm^{-1}$. Corresponding calculations that were also performed here for the excited $\tilde{a}^3B_1$ state of SiH_2 yield a singlet–triplet energy separation of

Table 3. Term values (in cm^{-1}) for the $\tilde{X}\,^1A_1$ electronic state of SiH_2.

$(v_1, v_2, v_3)^a$	$J_{K_a K_c}$	Observed[b]	O–C/MCI[c]	O–C/fitted[d]	Reference[e]
(0, 2, 0)	0_{00}	1978.153	9.629	1.316	(12)
(1, 0, 0)	0_{00}	2005.469	13.638	6.749	(12)
(1, 1, 0)	0_{00}	2952.7	13.6	3.0	(10)
(0, 3, 0)	0_{00}	2998.6	17.9	9.0	(10)
(1, 2, 0)	0_{00}	3907.4	24.4	−2.3	(10)
(2, 0, 0)	0_{00}	3923.3	20.1	−0.4	(10)
(0, 4, 0)	0_{00}	3976.8	18.5	4.6	(10)
(0, 0, 2)	0_{00}	3997.5	20.9	4.3	(10)
(0, 0, 1)	0_{00}	1992.816	1.541	−8.872	(12)
(0, 0, 0)	1_{10}	15.121	0.126	0.121	(12)
(0, 0, 0)	1_{01}	10.724	0.116	0.094	(12)
(0, 1, 0)	1_{01}	1009.42	2.64	1.20	(9)
(0, 0, 0)	1_{11}	11.801	0.066	0.078	(12)
(0, 1, 0)	1_{11}	1010.64	2.61	1.16	(9)
(3, 4, 0)	1_{11}	9487.14	61.08	−4.46	(15)
(1, 8, 0)	1_{11}	9522.23	63.21	−3.35	(15)
(2, 2, 2)	1_{11}	9592.28	47.80	−10.80	(15)
(0, 6, 2)	1_{11}	9612	44	−2	(15)
(0, 6, 2)	1_{11}	9641.18	44.32	−0.98	(15)
(1, 0, 4)	1_{11}	9670.99	63.58	−8.51	(15)
(0, 2, 4)	1_{11}	9696.98	50.84	7.95	(15)
(0,10, 0)	1_{11}	9735.38	34.26	13.29	(15)
(0, 0, 0)	2_{02}	29.700	0.261	0.231	(12)
(0, 0, 0)	2_{20}	45.564	0.354	0.354	(12)
(0, 1, 0)	2_{02}	1028.45	2.80	1.34	(9)
(0, 1, 0)	2_{00}	1045.42	2.93	1.46	(9)
(0, 0, 0)	2_{20}	29.930	0.239	0.223	(12)
(0, 1, 0)	2_{12}	1028.73	2.78	1.32	(9)
(0, 0, 0)	2_{21}	43.102	0.267	0.303	(12)
(0, 1, 0)	2_{21}	1042.87	2.85	1.38	(9)
(0, 0, 0)	2_{11}	39.879	0.418	0.352	(12)
(0, 1, 0)	2_{11}	1039.22	2.95	1.49	(9)
(3, 4, 0)	2_{11}	9517.72	62.16	−3.15	(15)
(1, 8, 0)	2_{11}	9553.58	68.83	−2.99	(15)
(2, 2, 2)	2_{11}	9623.17	50.35	−9.28	(15)
(0, 6, 2)	2_{11}	9642.23	44.09	−2.62	(15)
(0, 6, 2)	2_{11}	9671.18	44.75	−0.49	(15)
(1, 0, 4)	2_{11}	9698.96	65.52	−7.00	(15)
(0, 2, 4)	2_{11}	9725.16	49.65	−7.02	(15)
(0,10, 0)	2_{11}	9764.99	33.42	12.87	(15)

[a]The vibrational assignment of each state is that state which has the largest eigenvector coefficient from the output of the RENNER program using the fitted potentials.
[b]Experimentally derived term values.
[c]Residuals (observed–calculated) obtained using the MCI ab initio parameters from Table 1.
[d]Residuals (observed–calculated) obtained using the fitted parameters from Table 1.
[e]Reference for the experimentally derived ("Observed") term value.

$T_e(\tilde{a}) = 7140\ cm^{-1}$ (0.8852 eV). Experimentally (22), $T_0(\tilde{a})$ has been determined as being either 0.78 ± 0.03 eV or 0.91 ± 0.03 eV, and our result would suggest that the latter value is appropriate.

The two Renner states correlate with $Si(^1D) + H_2(\tilde{X}\,^1\Sigma_g^+)$ at dissociation (lowest dissociation channel) and hydrogen abstraction in the $\tilde{X}$ state leads to the higher dissociation channel: $SiH(\tilde{X}\,^2\Pi) + H(^2S)$. A wide variation in fluorescence lifetimes has been observed for individual rovibronic levels in the $\tilde{A}$ state that has been attributed to predissociation of these levels via random couplings to background levels of the $\tilde{a}\,^3B_1$ state (23). Some effort has been put recently into theoretical studies of the dissociation dynamics of the low-lying electronic states of SiH_2 including the triplet $\tilde{a}$ state (6). In these studies, both dissociation pathways of the ground electronic state have been found to be barrier free (without an energy maximum) whereas for the $\tilde{A}$

Table 4. Term values (in cm^{-1}) for the rotational level $J_{K_a K_c} = 1_{10}$ in various vibrational states of $\tilde{X}\,^1A_1$ SiH_2.

P^a	i^b	$(v_1, v_2, v_3)^c$	Observed[d]	O–C/MCI[e]	O–C/fitted[f]	P^a	i^b	$(v_1, v_2, v_3)^c$	Observed[d]	O-C/MCI[e]	O–C/fitted[f]
1	0	(0, 1, 0)	1014.14	2.66	1.22	8	8	(4, 0, 0)	(7578.04)	(7477.20)	(7578.49)
2	1	(0, 2, 0)	1993.62	9.93	1.47		7	(3, 2, 0)	7658.27	56.08	−4.17
	0	(1, 0, 0)	2020.82	13.59	6.83		6	(1, 6, 0)	7689.53	40.81	−1.02
3	1	(1, 1, 0)	2967.57	12.79	2.13		5	(2, 4, 0)	7753.27	44.77	0.91
	0	(0, 3, 0)	3014.28	17.86	9.00		4	(2, 0, 2)	7768.75	51.80	−5.06
4	3	(1, 2, 0)	3922.52	24.76	−2.64		3	(0, 4, 2)	7785.14	34.45	−4.63
	2	(2, 0, 0)	3939.45	20.36	0.64		2	(0, 8, 0)	7828.1	33.60	−0.53
	1	(0, 4, 0)	3991.33	17.28	3.16		1	(0, 0, 4)	7853.83	41.83	−1.06
	0	(0, 0, 2)	4011.73	20.22	3.85		0	(1, 6, 0)	7901.12	22.30	4.81
5	3	(1, 3, 0)	4877.49	26.13	−0.89	9	8	(4, 1, 0)	(8505.60)	(8401.54)	(8496.27)
	2	(2, 1, 0)	4904.98	25.71	0.91		7	(3, 3, 0)	8580.91	59.33	−2.53
	1	(0, 1, 2)	4956.74	18.01	−1.79		6	(1, 7, 0)	8612.59	46.95	−1.22
	0	(0, 1, 2)	4993.23	24.56	10.18		5	(0, 9, 0)	8682.95	47.99	−3.14
6	5	(3, 0, 0)	(5782.47)	(5729.31)	(5792.29)		4	(2, 1, 2)	8695.37	47.07	−2.96
	4	(1, 4, 0)	5823.36	30.77	0.14		3	(0, 5, 2)	8719.40	40.90	−1.85
	3	(2, 2, 0)	5863.23	30.55	2.15		2	(0, 1, 4)	8758.65	34.35	−9.30
	2	(1, 0, 2)	5905.36	30.78	−4.11		1	(0, 1, 4)	8798.85	38.04	10.02
	1	(1, 0, 2)	5931.12	32.90	8.84		0	(1, 7, 0)	8855.75	15.87	−1.95
	0	(1, 4, 0)	5970.53	27.50	12.32	10	11	(5, 0, 0)	9306.07	161.90	16.54
7	5	(3, 1, 0)	(6725.44)	(6671.64)	(6732.24)		10	(4, 2, 0)	(9424.55)	(9315.62)	(9406.03)
	4	(1, 5, 0)	6759.68	35.06	−0.75		9	(3, 4, 0)	9491.65	61.39	−4.10
	3	(2, 3, 0)	6812.43	34.00	1.98		8	(1, 8, 0)	9526.81	64.64	−3.33
	2	(1, 1, 2)	6845.77	28.76	−6.79		7	(3, 0, 2)	(9551.16)	(9475.72)	(9562.02)
	1	(1, 1, 2)	6887.15	33.00	8.48		6	(2, 2, 2)	9596.81	48.50	−10.43
	0	(1, 5, 0)	6939.03	25.87	9.41		5	(0, 6, 2)	9616.21	44.68	−2.86
							4	(0, 6, 2)	9644.74[g]	43.80	−1.48
							3	(1, 0, 4)	9675.08	64.57	−7.64
							2	(0, 2, 4)	9700.60	50.43	7.61
							1	(0,10, 0)	9739.40	33.97	13.14
							0	(1, 8, 0)	9800.78	4.58	−12.51

[a]Polyad quantum number $P = 2v_1 + v_2 + 2v_3$.
[b]Following ref. 15, we use i as a running number index within each polyad.
[c]The vibrational assignment of each state is that state which has the largest eigenvector coefficient from the output of the RENNER program using the fitted potentials.
[d]Experimentally derived term values from (15). The values in parentheses are calculated values from ref. 15.
[e]Residuals (observed–calculated) obtained using the MCI ab initio parameters from Table 1. For the levels that were not observed the MCI calculated value is placed here in parentheses.
[f]Residuals (observed–calculated) obtained using the fitted parameters from Table 1. For the levels that were not observed the calculated value obtained using the fitted potential is placed here in parentheses.
[g]Deperturbed from the triplet interaction (15).

state a very small energy maximum has been discovered in calculations at a medium accuracy level. To get reliable estimates of the basic energetics of these processes the relevant dissociation energies were calculated here at the theory level of the present study. For the two singlet states, the dissociation energies corresponding to the lower dissociation channel are 21 500 cm^{-1} and 5823 cm^{-1}, respectively, whereas for the higher dissociation channel of the $\tilde{X}$ state an energy of 27 545 cm^{-1} is obtained. The energy difference between the two dissociation limits of the $\tilde{X}$ state is thus 6045 cm^{-1}. This can be compared to the value of 6470 cm^{-1} that can be derived for this energy difference from the dissociation energies of H_2 and SiH, and the ^3P and ^1D term values for Si. Comparing the lower dissociation energies of the two singlet states with the corresponding energy barriers to linearity, we see that the barrier heights exceed the dissociation limits by several hundred wavenumbers.

The in-plane dipole moment components of the two singlet states were calculated relative to the molecular center of mass directly as expectation values from the previously iterated MR-CI wavefunctions for all different molecular geometries. The out-of-plane dipole transition moment was obtained at the CASSCF level from the individually optimized wavefunctions for each state, appying the restricted active space state interaction (RASSI) method of Malmqvist and Roos (24).

3. The potential energy and dipole moment surfaces

To calculate the rovibronic energies associated with the Renner-interacting $\tilde{X}\,^1A_1$ and $\tilde{A}\,^1B_1$ electronic states of SiH_2, we follow the approach described in refs. 25 and 26.

Table 5. Term values[h](in cm^{-1}) for the $\tilde{A}\,^1B_1$ state of SiH_2.

(v_1, v_2, v_3)	$J_{K_aK_c}$	Observed[b]	O–C/MCI[c]	O–C/fitted[d]	Reference[e]	(v_1, v_2, v_3)	$J_{K_aK_c}$	Observed[b]	O–C/MCI[c]	O–C/fitted[d]	Reference[e]
(0, 0, 0)	0_{00}	15 547.773	−1.304	−3.584	(7)	(0, 4, 0)	1_{10}	18 960.9	−72.5	−3.9	(18)
(0, 1, 0)	0_{00}	16 404.3	1.4	9.1	(18)	(0, 0, 0)	2_{11}	15 589.42	−1.76	−3.87	(7)
(0, 2, 0)	0_{00}	17 248.2	−17.7	2.9	(18)	(0, 1, 0)	2_{11}	16 447.8	−0.3	7.8	(18)
(0, 3, 0)	0_{00}	18 096.9	−33.1	1.9	(18)	(0, 2, 0)	2_{11}	17 297.5	−5.0	3.7	(18)
(0, 4, 0)	0_{00}	18 934.9	−55.6	−5.3	(18)	(0, 3, 0)	2_{11}	18 155.3	6.2	7.2	(18)
(0, 5, 0)	0_{00}	19 776	−69	−3	(18)	(0, 4, 0)	2_{11}	18 997.3	−55.0	−5.0	(18)
(0, 6, 0)	0_{00}	20 618.79	−77.24	4.06	(15)	(0, 5, 0)	2_{11}	19 852.1	−51.5	−4.0	(18)
(0, 7, 0)	0_{00}	21 467.89	−80.16	15.35	(15)	(0, 0, 0)	2_{21}	15 629.19	−3.61	−5.15	(7)
(0, 8, 0)	0_{00}	22 313	−97	26	(6)	(0, 1, 0)	2_{21}	16 492.1	−12.6	3.3	(18)
(1, 2, 0)	1_{10}	19 203.23	−49.91	−2.19	(8)	(0, 2, 0)	2_{21}	17 357.7	1.0	6.0	(18)
(1, 3, 0)	1_{10}	20 036.37	−64.49	2.56	(8)	(0, 3, 0)	2_{21}	18 227.2	−40.3	7.6	(18)
(1, 4, 0)	1_{10}	20 867.83	−76.54	9.85	(8)	(0, 4, 0)	2_{21}	19 097	−45	9	(18)
(1, 5, 0)	1_{10}	21 699.46	−82.51	23.26	(8)	(0, 0, 0)	2_{02}	15 573.7	−1.2	−3.4	(7)
(0, 0, 0)	1_{01}	15 556.44	−1.25	−3.53	(7)	(0, 0, 0)	2_{20}	15 629.26	−3.61	−5.15	(7)
(0, 1, 0)	1_{01}	16 412.4	0.8	8.6	(18)	(0, 1, 0)	2_{02}	16 428.7	−0.0	7.7	(18)
(0, 2, 0)	1_{01}	17 256.8	−17.7	2.9	(18)	(0, 1, 0)	2_{20}	16 492.3	−4.1	3.4	(18)
(0, 3, 0)	1_{01}	18 106.8	−31.8	3.2	(18)	(0, 2, 0)	2_{02}	17 274	−18	3	(18)
(0, 4, 0)	1_{01}	18 943.8	−55.3	−5.0	(18)	(0, 2, 0)	2_{20}	17 357.4	5.6	4.9	(18)
(0, 5, 0)	1_{01}	19 784.7	−69.2	−3.3	(18)	(0, 3, 0)	2_{02}	18 129.1	−26.8	8.4	(18)
(0, 6, 0)	1_{01}	20 629.6	−75.0	6.3	(18)	(0, 3, 0)	2_{20}	18 227.5	−40.0	10.8	(18)
(0, 0, 0)	1_{11}	15 569.83	−1.93	−3.96	(7)	(0, 4, 0)	2_{02}	18 960.9	−55.4	−5.0	(18)
(0, 1, 0)	1_{11}	16 429.6	1.1	9.2	(18)	(0, 4, 0)	2_{20}	19 096.9	−49.4	−7.6	(18)
(0, 2, 0)	1_{11}	17 277.6	−11.8	3.5	(18)	(0, 5, 0)	2_{02}	19 801.9	−69.7	−3.1	(18)
(0, 3, 0)	1_{11}	18 133.2	−3.3	4.4	(18)	(0, 6, 0)	2_{02}	20 644.7	−77.3	4.4	(18)
(0, 4, 0)	1_{11}	18 973.7	−62.9	3.3	(18)	(0, 0, 0)	2_{12}	15 586.03	−1.87	−3.91	(7)
(0, 5, 0)	1_{11}	19 832.7	−56.2	−7.6	(18)	(0, 1, 0)	2_{12}	16 443.2	−1.5	6.8	(18)
(0, 6, 0)	1_{11}	20 682.2	−52.7	7.7	(18)	(0, 2, 0)	2_{12}	17 293.9	−16.6	3.7	(18)
(0, 0, 0)	1_{10}	15 570.96	−1.89	−3.98	(7)	(0, 3, 0)	2_{12}	18 151.2	−14.0	5.4	(18)
(0, 1, 0)	1_{10}	16 430	0	8	(18)	(0, 4, 0)	2_{12}	18 992.5	−67.2	−2.5	(18)
(0, 2, 0)	1_{10}	17 278.1	−17.1	2.8	(18)	(0, 5, 0)	2_{12}	19 842.6	−73.0	−6.1	(18)
(0, 3, 0)	1_{10}	18 133.2	2.9	3.7	(18)	(0, 6, 0)	2_{12}	20 700.9	−63.9	0.5	(18)

[a]Term values are measured relative to the $(v_1, v_2, v_3)\,J_{K_aK_c} = (0, 0, 0)\,0_{00}$level of the $\tilde{X}\,^1A_1$ electronic state.
[b]Experimentally derived term values.
[c]Residuals (observed–calculated) obtained using the MCI ab initio parameters from Table 1.
[d]Residuals (observed–calculated) obtained using the fitted parameters from Table 1.
[e]Reference for the experimentally derived ("Observed") term value.

The rotational and vibrational motions in the two interacting Renner states are described in terms of a reference configuration with constant internuclear distances. This reference configuration is common for both electronic states and displacements due to stretching vibration are measured relative to it. As is customary (see (25–27)), since the two electronic surfaces are degenerate at linear configurations, we choose the bond lengths of the reference configuration to be those that minimize the electronic energy at linearity.

The Born–Oppenheimer potential energy function for the $\tilde{X}\,^1A_1$ electronic state is denoted by $V_-(\Delta r_{12}^{(\mathrm{ref})}, \Delta r_{32}^{(\mathrm{ref})}, \bar{\rho})$, and that for the $\tilde{A}\,^1B_1$ state is denoted $V_+(\Delta r_{12}^{(\mathrm{ref})}, \Delta r_{32}^{(\mathrm{ref})}, \bar{\rho})$, with

$$[1]\quad V_{\pm}(\Delta r_{12}^{(\mathrm{ref})}, \Delta r_{32}^{(\mathrm{ref})}, \bar{\rho}) = V_{\mathrm{ref}} + V_0^{(\pm)}(\bar{\rho}) + \sum_j F_j^{(\pm)} y_j^{(\mathrm{ref})} + \sum_{j\le k} F_{jk}^{(\pm)} y_j^{(\mathrm{ref})} y_k^{(\mathrm{ref})} + \sum_{j\le k\le m} F_{jkm}^{(\pm)} y_j^{(\mathrm{ref})} y_k^{(\mathrm{ref})} y_m^{(\mathrm{ref})} + \sum_{j\le k\le m\le n} F_{jkmn}^{(\pm)} y_j^{(\mathrm{ref})} y_k^{(\mathrm{ref})} y_m^{(\mathrm{ref})} y_n^{(\mathrm{ref})} + \ldots$$

Table 6. Transition wavenumbers and band origins (in cm^{-1}) of the $\tilde{A} \rightarrow \tilde{X}$ transitions of SiD_2.

(v_1'', v_2'', v_3'')	(v_1', v_2', v_3')	Observed	O–C[c]
(0,0,0)	(0,0,0)	15 539.875[a]	−4.402
(0,1,0)	(0,0,0)	16 158.427[a]	1.735
(0,2,0)	(0,0,0)	16 774.440[a]	1.034
(0,3,0)	(0,0,0)	17 385[b]	−1
(0,4,0)	(0,0,0)	17 996[b]	−6
(0,5,0)	(0,0,0)	18 603[b]	−11
(0,6,0)	(0,0,0)	19 201[b]	−21
(0,7,0)	(0,0,0)	19 803[b]	−20
(0,8,0)	(0,0,0)	20 401[b]	−16
(0,9,0)	(0,0,0)	20 998[b]	−10
(0,10,0)	(0,0,0)	21 599[b]	−1
(0,1,0)	(0,1,0)	15 435.428[a]	−0.945
(0,2,0)	(0,2,0)	15 338.309[a]	1.006

[a]Experimentally derived band origins from ref. 14.
[b]Experimental transition wavenumbers for the rovibronic transitions $J_{K_a K_c} = 0_{00}(\tilde{A}) \rightarrow 1_{10}(\tilde{X})$ from ref. 13.
[c]Residuals (observed–calculated) obtained using the fitted parameters from Table 1.

where j, k, m, and n = 1 or 3. $V_-(\Delta r_{12}^{(\mathrm{ref})}, \Delta r_{32}^{(\mathrm{ref})}, \bar{\rho})$ and $V_+(\Delta r_{12}^{(\mathrm{ref})}, \Delta r_{32}^{(\mathrm{ref})}, \bar{\rho})$ depend on the stretching displacements

$$[2] \qquad \Delta r_{j2}^{(\mathrm{ref})} = r_{j2} - r_{j2}^{(\mathrm{ref})}$$

where r_{j2} is the instantaneous value of the distance between the proton labeled j (= 1 or 3) and the Si nucleus (labeled 2), and $r_{j2}^{(\mathrm{ref})}$ is the reference value of this quantity. As mentioned above, the $r_{j2}^{(\mathrm{ref})}$ are taken as the optimum bond lengths at linearity. In eq. [1],

$$[3] \qquad y_j^{(\mathrm{ref})} = 1 - \exp\left(-a\Delta r_{j2}^{(\mathrm{ref})}\right)$$

and $\bar{\rho} = \pi - \angle(\mathrm{HSiH})$, where $\angle(\mathrm{HSiH})$ is the instantaneous value of the bond angle. The functions $V_0^{\pm}(\bar{\rho})$ and $F_{jk\ldots}^{\pm}(\bar{\rho})$ are expressed as cosine series:

$$[4] \qquad V_0^{\pm}(\bar{\rho}) = \sum_{i=1}^{8} f_0^{(i,\pm)}(1 - \cos\bar{\rho})^i$$

and

$$[5] \qquad F_{jk\ldots}^{\pm}(\bar{\rho}) = f_{jk\ldots}^{(0)} + \sum_{i=1}^{N} f_{jk\ldots}^{(i,\pm)}(1 - \cos\bar{\rho})^i$$

where $f_0^{(i,\pm)}$, $f_{jk\ldots}^{(0)}$ and $f_{jk\ldots}^{(i,\pm)}$ are expansion coefficients. In eq. [5], the expression for $F_j^{\pm}(\bar{\rho})$ has $N = 4$, that for $F_{jk}^{\pm}(\bar{\rho})$ has $N = 3$, $F_{jkl}^{\pm}(\bar{\rho})$ has $N = 2$, and $F_{jklm}^{\pm}(\bar{\rho})$ has $N = 1$. Since the expansion coefficients $f_{jk\ldots}^{(0)}$ are chosen to be common for both electronic states, the potentials given by eq. [1] are degenerate for linear configurations; the term V_{ref} in eq. [1] is the energy for $\bar{\rho} = 0$, and $r_{12} = r_{32} = r_{12}^{(\mathrm{ref})}$, and it is also common for the two potential surfaces.

We describe the molecular dipole moment in terms of its components along three axes xqp (taken to form a right-handed axis system with origin in the nuclear center of mass) that are attached directly to the instantaneous nuclear configuration of the molecule (see Fig. 1 of ref. 28). For SiH_2, the q axis bisects the bond angle $\angle(\mathrm{HSiH})$ and is directed so that the q coordinates of the H nuclei 1 and 3 are positive. The p axis is perpendicular to the q axis and its direction is such that the p coordinate of nucleus 3 is positive, and the x axis is perpendicular to the molecular plane.

The expressions for the intensities of individual rovibronic transitions within the two Renner-degenerate electronic states are given in ref. 29. These intensities depend on electronic dipole moment and transition moment surfaces. We denote the electronic wavefunction for the $\tilde{X}\,{}^1A_1$ state as $\psi_{\mathrm{elec}}^{(-)}$, and that for the $\tilde{A}\,{}^1B_1$ state as $\psi_{\mathrm{elec}}^{(+)}$. In this notation we obtain the following non vanishing dipole and transition moments:

$$[6] \qquad \bar{\mu}_p^{(\sigma)}(\Delta r_{12}^{(\mathrm{ref})}, \Delta r_{32}^{(\mathrm{ref})}, \bar{\rho}) = \langle\psi_{\mathrm{elec}}^{(\sigma)}|\mu_p|\psi_{\mathrm{elec}}^{(\sigma)}\rangle_{\mathrm{el}}$$

$$[7] \qquad \bar{\mu}_q^{(\sigma)}(\Delta r_{12}^{(\mathrm{ref})}, \Delta r_{32}^{(\mathrm{ref})}, \bar{\rho}) = \langle\psi_{\mathrm{elec}}^{(\sigma)}|\mu_q|\psi_{\mathrm{elec}}^{(\sigma)}\rangle_{\mathrm{el}}$$

where, in eqs. [6] and [7], $\sigma = -$ or $+$, and

$$[8] \qquad \bar{\mu}_x^{(-+)}(\Delta r_{12}^{(\mathrm{ref})}, \Delta r_{32}^{(\mathrm{ref})}, \bar{\rho}) = \langle\psi_{\mathrm{elec}}^{(-)}|\mu_x|\psi_{\mathrm{elec}}^{(+)}\rangle_{\mathrm{el}}$$

where, in eqs. [6]–[8], the subscript "el" indicates that integration is over the electronic coordinates only.

The functions $\bar{\mu}_p^{(\sigma)}$ and $\bar{\mu}_q^{(\sigma)}$ are represented as (see ref. 28)

$$[9] \qquad \bar{\mu}_p^{(\sigma)}(\Delta r_{12}^{(\mathrm{ref})}, \Delta r_{32}^{(\mathrm{ref})}, \bar{\rho}) = \mu_0^{(p;\sigma)}(\bar{\rho}) + \sum_j \mu_j^{(p;\sigma)}(\bar{\rho})\Delta r_{j2}^{(\mathrm{ref})} + \sum_{j\le k} \mu_{jk}^{(p;\sigma)}(\bar{\rho})\Delta r_{j2}^{(\mathrm{ref})}\Delta r_{k2}^{(\mathrm{ref})} + \sum_{j\le k\le m} \mu_{jkm}^{(p;\sigma)}(\bar{\rho})\Delta r_{j2}^{(\mathrm{ref})}\Delta r_{k2}^{(\mathrm{ref})}\Delta r_{m2}^{(\mathrm{ref})} + \sum_{j\le k\le m\le n} \mu_{jkmn}^{(p;\sigma)}(\bar{\rho})\Delta r_{j2}^{(\mathrm{ref})}\Delta r_{k2}^{(\mathrm{ref})}\Delta r_{m2}^{(\mathrm{ref})}\Delta r_{n2}^{(\mathrm{ref})}$$

and

$$[10]\quad \bar{\mu}_q^{(\sigma)}(\Delta r_{12}^{(\mathrm{ref})}, \Delta r_{32}^{(\mathrm{ref})}, \bar{\rho}) = \sin\bar{\rho}\Bigg[\mu_0^{(q;\sigma)}(\bar{\rho}) + \sum_j \mu_j^{(q;\sigma)}(\bar{\rho})\Delta r_{j2}^{(\mathrm{ref})} + \sum_{j\le k} \mu_{jk}^{(q;\sigma)}(\bar{\rho})\Delta r_{j2}^{(\mathrm{ref})}\Delta r_{k2}^{(\mathrm{ref})} + \sum_{j\le k\le m} \mu_{jkm}^{(q;\sigma)}(\bar{\rho})\Delta r_{j2}^{(\mathrm{ref})}\Delta r_{k2}^{(\mathrm{ref})}\Delta r_{m2}^{(\mathrm{ref})} + \sum_{j\le k\le m\le n} \mu_{jkmn}^{(q;\sigma)}(\bar{\rho})\Delta r_{j2}^{(\mathrm{ref})}\Delta r_{k2}^{(\mathrm{ref})}\Delta r_{m2}^{(\mathrm{ref})}\Delta r_{n2}^{(\mathrm{ref})}\Bigg]$$

with $j, k, m, n = 1$ or 3. The angle-dependent coefficients are given by

$$[11]\quad \mu_{jk\ldots}^{(w;\sigma)}(\bar{\rho}) = \sum_{i=0}^{N} w_{jk\ldots}^{(i;\sigma)}(1-\cos\bar{\rho})^i$$

with $w = p$ or q. The function $\mu_0^{(w;\sigma)}(\bar{\rho})$ has $N = 8$, $\mu_j^{(w;\sigma)}(\bar{\rho})$ has $N = 4$, $\mu_{jk}^{(w;\sigma)}(\bar{\rho})$ has $N = 3$, $\mu_{jkm}^{(w;\sigma)}(\bar{\rho})$ has $N = 2$ and $\mu_{jkmn}^{(w;\sigma)}(\bar{\rho})$ has $N = 1$.

The function $\bar{\mu}_x^{(-+)}$ is parameterized as

$$[12]\quad \bar{\mu}_x^{(-+)}(\Delta r_{12}^{(\mathrm{ref})}, \Delta r_{32}^{(\mathrm{ref})}, \bar{\rho}) = \sin\bar{\rho}\Bigg[\mu_0^{(x;-+)}(\bar{\rho}) + \sum_j \mu_j^{(x;-+)}(\bar{\rho})\Delta r_{j2}^{(\mathrm{ref})} + \sum_{j\le k} \mu_{jk}^{(x;-+)}(\bar{\rho})\Delta r_{j2}^{(\mathrm{ref})}\Delta r_{k2}^{(\mathrm{ref})} + \sum_{j\le k\le m} \mu_{jkm}^{(x;-+)}(\bar{\rho})\Delta r_{j2}^{(\mathrm{ref})}\Delta r_{k2}^{(\mathrm{ref})}\Delta r_{m2}^{(\mathrm{ref})} + \sum_{j\le k\le m\le n} \mu_{jkmn}^{(x;-+)}(\bar{\rho})\Delta r_{j2}^{(\mathrm{ref})}\Delta r_{k2}^{(\mathrm{ref})}\Delta r_{m2}^{(\mathrm{ref})}\Delta r_{n2}^{(\mathrm{ref})}\Bigg]$$

with

$$[13]\quad \mu_{jk\ldots}^{(x;-+)}(\bar{\rho}) = \sum_{i=0}^{N} x_{jk\ldots}^{(i;-+)}(1-\cos\bar{\rho})^i$$

where the number of summation terms N is given exactly as for eq. [11].

For SiH_2, relations exist between the expansion coefficients in eqs. [11] and [13], so that the functions $\bar{\mu}_q^{(\sigma)}$ and $\bar{\mu}_x^{(-+)}$ are unchanged under the interchange of the two protons, whereas the function $\bar{\mu}_p^{(\sigma)}$ is antisymmetric under this operation.

4. Fitting to the ab initio points

The analytical expression for the potential energy function defined in eqs. [1]–[5] contains as adjustable parameters the coefficients $f_0^{(i,\pm)}$ in eq. [4], and $f_{jk\ldots}^{(0)}$ and $f_{jk\ldots}^{(i,\pm)}$ in eq. [5], and the parameters a in eq. [3] and V_{ref} in eq. [1]. We aim to determine values of these parameters in fittings to the MCI ab initio points. Since we define the reference bond length $r_{j2}^{(\mathrm{ref})}$ to be equal to the optimum bond length at linearity, this parameter can also be adjusted in the fittings.

Attempts to determine the parameter a in the fittings led to divergence of the least-squares-fitting procedure and so we had to constrain it. It was constrained to the value $a = 1.58$ Å^{-1} determined by fitting to the ab initio energies of the points with $r_{32} = r_{12}$ and $\bar{\rho} = 90°$ (close to the equilibrium value of $\bar{\rho}$ in the $\tilde{X}\,^1A_1$ electronic state). The energies in these points depend only on r_{12} and we fitted a Morse potential

$$[14]\quad V_{\mathrm{Morse}}(r_{12}) = V_{\mathrm{e}} + f_{11}^{(0)}\left[1 - e^{-a\Delta r_{12}^{(\mathrm{ref})}}\right]^2$$

through them, thus determining the value of a.

We carried out initial fittings to the ab initio points and used the resulting parameter values as input for the program RENNER (25, 26, 29), which calculates rovibronic energies and intensities for Renner-degenerate electronic states of triatomic molecules. This calculation produced values of the lowest $\tilde{A}\,^1B_1$ $(0, v_2, 0)$ energies that were consistently about 150 cm^{-1} higher than their respective experimental counterparts. This type of effect is often encountered in ab initio calculations of rovibronic energies associated with Renner-degenerate electronic states; it simply indicates that the $\tilde{A}$-state potential energy surface lies too high by 150 cm^{-1} relative to the $\tilde{X}$-state surfaces. To improve the agreement with experiment of the the rovibronic energies calculated from the ab initio results, we subtracted 150 cm^{-1} from all the $\tilde{A}$-state ab initio energies, and fitted the analytical expression for the potential energy function defined in eqs. [1]–[4] through these corrected $\tilde{A}$-state ab initio points and through the $\tilde{X}$-state points. The two analytical surfaces obtained in this fitting have barriers to linearity approximately 150 cm^{-1} lower than obtained in the initial fitting. In the final fitting, we used 250 ab initio points as input and we could usefully vary 34 potential parameters. The standard deviation was 20 cm. The optimized parameter values and their

Table 7. The composition (in percentage points[a]) of the rotational level $J_{K_aK_c} = 1_{10}$, in the polyad states with $P = 10$ of $\tilde{X}\,^1A_1$ SiH_2, in terms of vibrational basis functions (v_1, v_2, v_3).

$i = (v_1, v_2, v_3)$	0	1	2	3	4	5	6	7	8	9	10	11
(5,0,0)								6.8			1.5	85.8
(3,0,2)			2.4	31.2				54.0				6.5
(1,0,4)			3.2	56.1				34.8				1.1
(4,2,0)					1.2	4.4	4.4			1.7	63.0	
(2,2,2)		6.5	9.7		3.6	18.3	28.5			1.7	12.2	
(0,2,4)		14.4	39.6	8.4	14.2	8.2	1.1					
(3,4,0)		5.2			7.7		1.5		3.2	45.9		
(1,4,2)	1.5	13.7			9.9		23.6		17.4	6.7		
(2,6,0)	6.4	5.6	4.5			8.9	1.6		19.1	12.6		
(0,6,2)	5.5	4.5	8.9		35.7	20.0						
(1,8,0)	21.9					4.4	7.5		21.9	4.4		
(0,10,0)	20.3	15.9	10.7		1.7	7.7	9.7		7.8	1.1		
$\sum^b$	55.7	65.8	79.1	95.6	73.9	71.8	77.9	95.6	69.4	74.2	76.7	93.4

[a]Contributions that are less than 1% are omitted.
[b]Sum of percentage contributions for each state i within the polyad.

Table 8. The polyad composition (in percentage points[a]) of the rotational level $J_{K_aK_c} = 1_{10}$ in the polyad states with $P = 10$ of $\tilde{X}\,^1A_1$ SiH_2.

$i = P$	0	1	2	3	4	5	6	7	8	9	10	11
8									4.4	3.4		
9	18.0	12.1	3.0		7.1	6.4	3.8		5.4	4.3	8.6	2.6
10	55.7	65.8	79.1	95.6	73.9	71.8	77.9	95.6	69.4	74.2	76.7	93.4
11	5.4	2.3	3.1		2.9	1.8			1.7	2.3	4.6	1.7
12	9.1	4.1	2.5		3.5	5.1	6.0		9.3	7.2	3.8	
13	3.4										1.5	

[a]Contributions that are less than 1% are omitted.

standard errors are given in Table 1 under the heading "MCI ab initio".

The MCI ab initio fitted analytical potential functions (with the barrier to linearity lowered by 150 cm^{-1} as discussed above) are such that the equilibrium geometry (r_e, α_e) is (1.518 Å, 92.4°) for the $\tilde{X}$ state and (1.487 Å, 122.9°) for the $\tilde{A}$ state. The barrier heights at linearity in these functions are 22 139.2 and 6612.8 cm^{-1}, respectively, for the $\tilde{X}$ and $\tilde{A}$ states, so that $T_e(\tilde{A}) = 15\,526.4$ cm^{-1}.

For the dipole moment and transition moment surfaces we obtain values for the $p^{(i;\sigma)}_{jk...}$, $q^{(i;\sigma)}_{jk...}$, and $x^{(i;-+)}_{jk...}$ parameters by fitting eqs. [9]–[13] through the ab initio dipole moment values. The results of the fittings (parameter values, standard errors, and the standard deviations of the fittings) are given in Table 2.

From the ab initio calculation we determine that the dipole moment for the $\tilde{X}$ state at its equilibrium configuration is 0.14 D, and for the $\tilde{A}$ state at its equilibrium configuration it is 0.01 D. The $\tilde{A} - \tilde{X}$ transition moment at the equilibrium geometry of the $\tilde{X}$ state is calculated to be 1.21 D.

5. Rovibronic energy calculations

In the RENNER calculations, the eigenvalues for the rovibronic Hamiltonian $\hat{H}_{Renner}$ were obtained by diagonalization of the matrix representation of $\hat{H}_{Renner}$ in the basis set $|v_2^{(\eta)}, K\rangle$ $|N_{vib}^{(\eta)}, \Gamma_{vib}^{(\eta)}\rangle$ $|\eta; NJSKM_J\tau\rangle$ defined in ref. 25. We used the 27 lowest bending basis functions $|v_2^{(\eta)}, K\rangle$ for both electronic states for every K block (where $K \leq J$). The $\tilde{X}\,^1A_1$ electronic state basis set included the $N_A = 20$ lowest stretching functions $|N_{vib}^{(\eta)}, A_1\rangle$ of A_1 symmetry and the $N_B = 15$ lowest stretching functions $|N_{vib}^{(\eta)}, B_2\rangle$ of of B_2 symmetry. For the $\tilde{A}\,^1B_1$ state we used $N_A = 15$ and $N_B = 10$ stretching functions. These stretching functions were constructed from Morse oscillator functions $|n_1\rangle$ $|n_3\rangle$ with $n_1 + n_3 \leq N_{stretch} = 17$.

Rovibronic energies calculated with the RENNER program from the ab initio parameters in Table 1 are compared with experimental values for SiH_2 in Tables 3–5 under the heading "O–C/MCI". In Table 3, the comparison is made for $J \leq 2$ term values for vibrational states in the $\tilde{X}\,^1A_1$ electronic state. In Table 4, the comparison is made for the extensive set of $\tilde{X}\,^1A_1$ term values (which all have $J_{K_aK_c} = 1_{10}$) obtained experimentally in the recent stimulated emission pumping study by Ishikawa et al. (15). The energies in Table 4 are labeled by the polyad quantum number

$$P = 2v_1 + v_2 + 2v_3.$$

Since, for $\tilde{X}\,^1A_1$ SiH_2, the three harmonic vibrational wavenumbers ω_1, ω_2, and ω_3 approximately satisfy the relation $\omega_1 =$

Table 9. Predicted term values T_{calc} (in cm^{-1}) for the rotational level $J_{K_aK_c} = 1_{10}$ in the polyad states with $P = 11$ and 12 of $\tilde{X}\,^1A_1$ SiH_2.

P	(v_1, v_2, v_3)	T_{calc}	P	(v_1, v_2, v_3)	T_{calc}
11	(5, 1, 0)	10 181.37	12	(6, 0, 0)	10 923.17
	(4, 3, 0)	10 307.98		(5, 2, 0)	11 067.05
	(3, 5, 0)	10 399.74		(4, 4, 0)	11 202.28
	(1, 5, 2)	10 439.36		(4, 0, 2)	11 273.94
	(3, 1, 2)	10 464.93		(3, 6, 0)	11 295.62
	(2, 3, 2)	10 515.08		(1, 6, 2)	11 341.27
	(0, 7, 2)	10 536.76		(3, 2, 2)	11 360.91
	(0, 7, 2)	10 564.67		(2, 4, 2)	11 414.06
	(1, 1, 4)	10 591.10		(0, 4, 4)	11 446.39
	(0, 3, 4)	10 611.07		(2, 0, 4)	11 474.45
	(0,11, 0)	10 661.68		(0, 8, 2)	11 477.20
	(1, 9, 0)	10 762.55		(1, 2, 4)	11 492.85
				(0, 4, 4)	11 525.16
				(0, 0, 6)	11 560.37
				(0,12, 0)	11 592.15
				(1,10, 0)	11 704.90

Table 10. Term values (in cm^{-1}) with K_a=J for $\tilde{A}\,^1B_1$ SiH_2.

(v_1, v_2, v_3)	$J_{K_aK_c}$	Observed[a]	O–C[b]
(0, 1, 0)	3_{31}	16 596.8	1.08
(0, 2, 0)	3_{31}	17 480.3	0.28
(0, 3, 0)	3_{31}	18 368.2	0.58
(0, 4, 0)	3_{31}	19 261.5	−6.43
(0, 1, 0)	4_{41}	16 739.3	−1.87
(0, 2, 0)	4_{41}	17 638.9	4.63
(0, 3, 0)	4_{41}	18 547.7	−5.08
(0, 4, 0)	4_{41}	19 462.3	−12.98
(0, 1, 0)	5_{51}	16 913.7	−6.38
(0, 2, 0)	5_{51}	17 832.1	−8.44
(0, 3, 0)	5_{51}	18 760.6	−8.31
(0, 4, 0)	5_{51}	19 697.9	0.37

[a]From ref. 15.
[b]Observed–calculated obtained using the fitted parameters from Table 1.

$2\omega_2 = \omega_3$, vibrational states with a common value of P will be close in energy and form polyads labeled by $P = 0, 1, 2, 3, \ldots$. Within each polyad the energies in Table 4 are labeled by the running number index i as in ref. 15. In Table 5, we make the comparison for $J \leq 2$ term values in the $\tilde{A}\,^1B_1$ state.

The energies calculated using RENNER with the ab initio parameters in Table 1 reproduce the experimental energies for SiH_2 in Tables 3–5 with a root-mean-square deviation of 41.7 cm^{-1}. It is noticeable that while the agreement between theory and experiment is fairly good for low-lying states, there are substantial deviations for the highly excited states, in particular for the $\tilde{X}\,^1A_1$ -levels characterized experimentally by Ishikawa et al. (15) in stimulated emission pumping experiments. To analyze theoretically these highly excited states and, hopefully, explain the intensities of the emission spectra observed by Ishikawa et al. (15), we have refined the potential energy surfaces of $\tilde{X}\,^1A_1$ and $\tilde{A}\,^1B_1$ SiH_2 in a least-squares fitting to the available low-J experimental data. This refinement is the subject of the following section.

Table 11. Term values (in cm^{-1}) for the rotational level $J_{K_aK_c} = 1_{10}$ in the polyad states with $P = 10$ of $\tilde{X}\,^1A_1$ SiH_2.

Observed (15)	i	Calculated term value[a]	i	Alternative term value[b]
9800.78	0	9813.29	0	9807.74
9739.40	1	9726.26	1	9731.52
9700.60	2	9692.99	2	9708.08
9675.08	3	9682.72	3	9673.94
9644.74	4	9646.22	4	9657.43
9616.21	5	9619.07	5	9621.92
9596.81	6	9607.24	6	9592.11
	7	9562.02	7	9551.47
9526.81	8	9530.14	8	9527.37
9491.65	9	9495.75	9	9494.86
	10	9406.03		
9306.07[c]	11	9289.53	10	9308.14
			11	9132.95

[a]Obtained using the fitted potentials with the parameters from Table 1.
[b]The result using the alternative potentials (see text).
[c]This would be assigned as $i = 11$ using our fitted potentials, but as $i = 10$ using the alternative potentials.

6. Refinement of the potentials

The adjustment of potential energy parameters in a fitting to experimental data can sometimes lead to an unrealistically shaped potential energy surface (PES). To constrain the shape of the PES during the fitting process we performed a simultaneous fitting of the potential parameters both to the observed data and to ab initio energies. By introducing the ab initio energies as input data for the fitting, we can constrain the fitted potential energy surface to be close to the initial ab initio one. This approach has been discussed in detail in ref. 30 and we give a brief outline here.

The ab initio parameters from Table 1 were first used to generate a grid of ab initio energy points that we used in the simultaneous fitting procedure. Some of these points involved extrapolation outside the region of the ab initio calculation and they were given low weight. In the simultaneous fitting procedure we must decide on a particular value for the ratio of the weights used for the experimental data (W_i^{exp}) to that used for the ab initio points (W_i^{points}), and in this work the weight for the data was taken to be 5.5 times larger than that on the ab initio points.

In the refinement we first fitted to levels with $J \leq 1$ for SiH_2 (excluding the levels from the 10th polyad (15) in the $\tilde{X}$ state). We added levels with $J = 2$, and levels for SiD_2 (see Table 6) as we achieved reasonable agreement with the experimental data. Finally, the energy levels of the $P = 10$ polyad were included; the vibrational assignments of these levels were very sensitive

Fig. 1. Probability distributions $f(\rho)$ for the rotational level $J_{K_aK_c} = 1_{10}$ in the polyad states with $P = 10$ of $\tilde{X}\,^1A_1$ SiH_2. The energies of these states are given in Table 11.

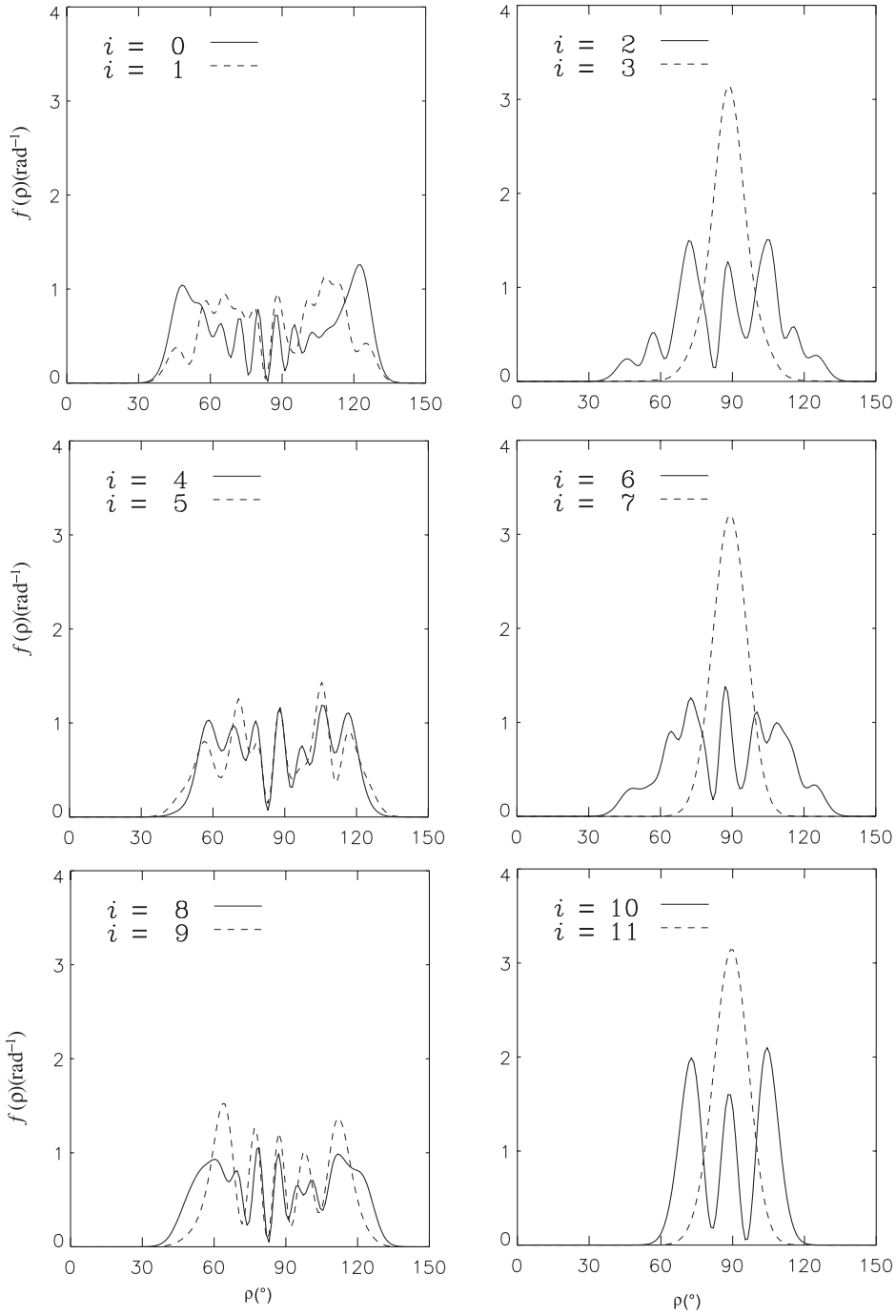

to any parameter change. The resultant parameters are listed in column three of Table 1, and the residuals "O–C/fitted" are given in Tables 3–6. The vibronic assignment of each state is that state which has the largest eigenvector coefficient from the output of the RENNER program. These assignments are of help in understanding the polyad structure of the vibrational levels in the ground electronic state. For example, one can learn from Table 4 that for the ground electronic state the highest level in every Pth polyad is the level $(v_1, v_2, v_3) = (1, P - 2, 0)$ for $P > 5$. In Table 7, we show the percentages of each (v_1,v_2,v_3) state that occurs in each of the $P = 10$ polyad states, and in Table 8, we show the percentages of neighboring polyads basis functions that are mixed into the $P = 10$ polyad states.

In Table 9 we give the predicted term values for the $J_{K_aK_c} = 1_{10}$ levels of the polyads having $P = 11$ and 12, and in Table 10 we compare calculated and observed $\tilde{A}$-state levels hav-

Fig. 2. Probability distributions $f(\rho)$ for the the rotational level $J_{K_aK_c} = 0_{00}$ in the $7\nu_2$ state of $\tilde{A}\,^1B_1$ SiH_2.

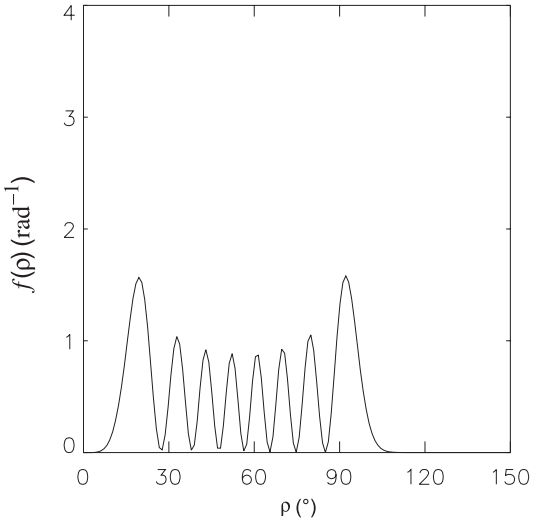

Fig. 3. Probability distributions $f(\rho)$ for the rotational level $J_{K_aK_c} = 0_{00}$ in the (*a*) ν_1 and (*b*) $2\nu_2$ states of $\tilde{X}\,^1A_1$ SiH_2.

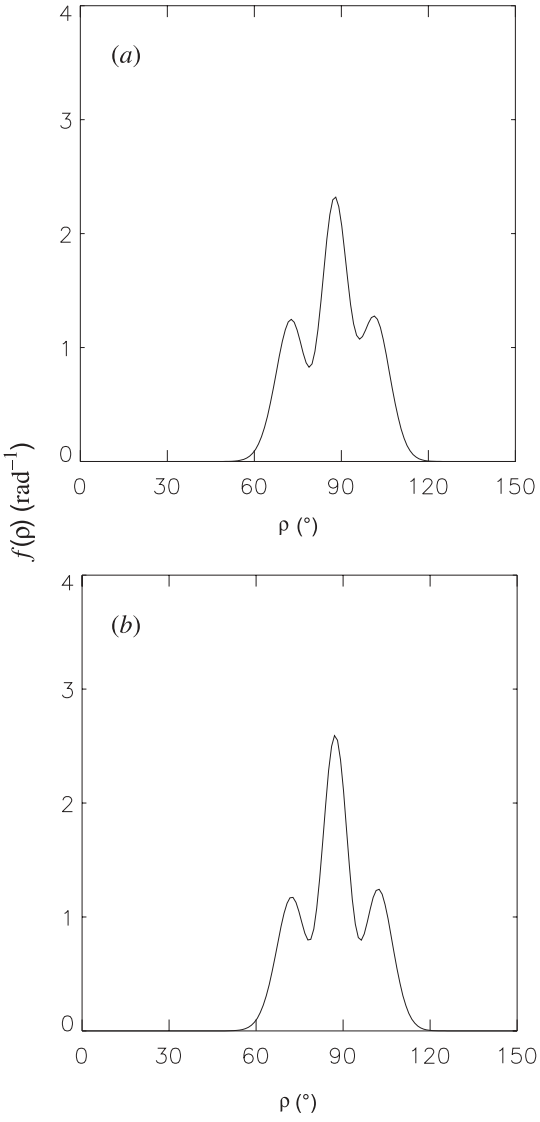

Fig. 4. The upper emission spectrum is the observed $P = 10$ spectrum (15) (see footnote 3), and the lower stick spectrum is the simulation using our fitted potentials and ab initio dipole moment and transition moment surfaces. The doublet in the observed spectrum at around 9645 cm^{-1} results from the presence of a triplet state perturber that we do not include in our simulation.

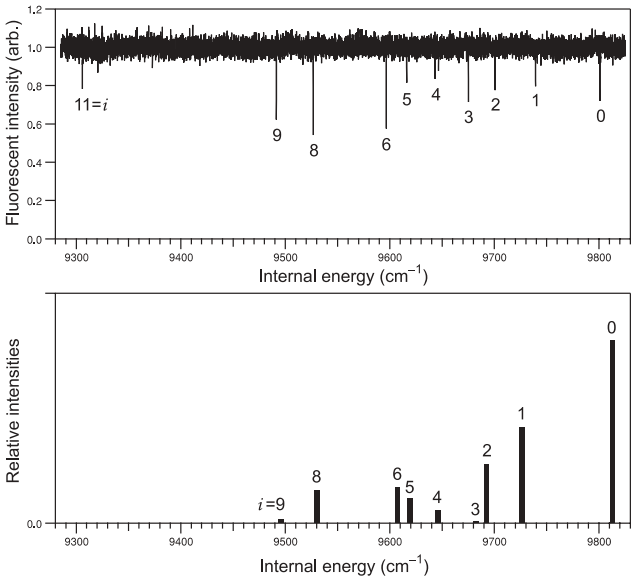

Fig. 5. The upper emission spectrum is the observed $P = 10$ spectrum (15) (see footnote 3), and the lower stick spectrum is the simulation using our alternative potentials (see text) with the ab initio dipole moment and transition moment surfaces. The reproduction of the intensities is worse than that in Fig. 4 and this leads us to discard the alternative potentials.

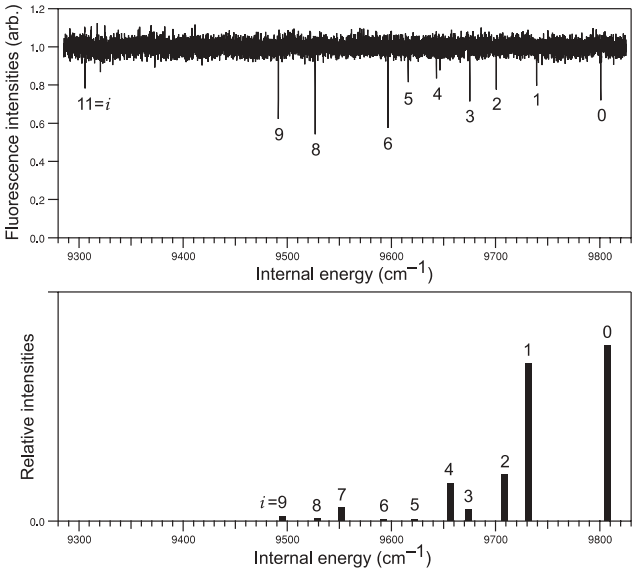

ing higher values of J and K_a. This latter comparison is a check that our calculation treats the Renner effect appropriately in higher angular momentum states.

The observed data, for $J = 0$, 1, and 2, are reproduced with a root-mean-square error of 5.8 cm^{-1} for the $\tilde{X}\,^1A_1$ state and

7.3 cm^{-1} for the $\tilde{A}\,^1B_1$ state. The energies of the ab initio points are reproduced with root-mean-square error of 30.0 cm^{-1} for the $\tilde{X}\,^1A_1$ state and 42.0 cm^{-1} for the $\tilde{A}\,^1B_1$ state.

The fitted potentials are such that the equilibrium geometry (r_e, α_e) is (1.518 Å, 92.4°) for the $\tilde{X}$ state and (1.486 Å, 123.0°) for the $\tilde{A}$ state. The barrier heights at linearity are obtained from the fitted potentials as 21 882.4 and 6340.6 cm^{-1}, respectively, for the $\tilde{X}$ and $\tilde{A}$ states, so that $T_e(\tilde{A})$ = 15 541.8 cm^{-1}.

7. Rovibronic wavefunctions and probability density functions

An eigenfunction obtained from the rovibronic RENNER calculation is given as a superposition of basis functions, and we can write it as

$$[15]\quad \psi^{(i,J,M_J,S,\Gamma_{evr};\tau)}_{evr-ns} = \Phi_{ns} \sum_{\eta=a,b} \sum_{N=|J-S|}^{J+S} \sum_{K=0}^{N} \sum_{v_2^{(\eta)},N_{vib}^{(\eta)},\Gamma_{vib}^{(\eta)}} c^{(i,J,M_J,S,\Gamma_{evr},\tau)}_{\eta,N,K,v_2^{(\eta)},N_{vib}^{(\eta)},\Gamma_{vib}^{(\eta)}} \times \Phi_{v_2^{(\eta)},K}(\rho)\, \Phi_{N_{vib}^{(\eta)},\Gamma_{vib}^{(\eta)}}(r_{12},r_{32})\, |\eta; NJSKM_J\tau\rangle$$

where the $c^{(i,J,M_J,S,\Gamma_{evr},\tau)}_{\eta,N,K,v_2^{(\eta)},N_{vib}^{(\eta)},\Gamma_{vib}^{(\eta)}}$ are expansion coefficients, and the functions $\Phi_{v_2^{(\eta)},K}(\rho)$ (called $|v_2^{(\eta)}, K\rangle$ in ref. 25) and $\Phi_{N_{vib}^{(\eta)},\Gamma_{vib}^{(\eta)}}(r_{12}, r_{32})$ (called $|N_{vib}^{(\eta)}, \Gamma_{vib}^{(\eta)}\rangle$ in ref. 25) are basis functions describing the bending and stretching motions, respectively. $\Phi_{v_2^{(\eta)},K}(\rho)$ depends on the bending coordinate ρ which is almost, but not quite, equal to $\bar{\rho}$. The rigid-bender functions $\Phi_{v_2^{(\eta)},K}(\rho)$, and Morse oscillator stretching functions $\Phi_{N_{vib}^{(\eta)},\Gamma_{vib}^{(\eta)}}(r_{12}, r_{32})$, are defined in ref. 25; $v_2^{(\eta)}$ is the bending quantum number appropriate for a bent molecule (See section 13.4.1 and eqs. [13]–[177] of ref. 1). $\Gamma_{vib}^{(\eta)}$ is the irreducible representation spanned by the function $\Phi_{N_{vib},\Gamma_{vib}^{(\eta)}}$ in the molecular symmetry group of the molecule and, $N_{vib}^{(\eta)}$ = 1, 2, 3, … numbers the functions with a given $\Gamma_{vib}^{(\eta)}$ in order of ascending energy. For SiH_2, the molecular symmetry group is C_{2v}(M) (1) and $\Gamma_{vib}^{(\eta)} = A_1$ or B_2. The basis functions $|\eta; NJSKM_J\tau\rangle$ describe the motion of the electrons, the electron spin, and the rotational motion (where $K = K_a$). These functions are given as

$$[16]\quad |a; NJSKM_J\tau\rangle = \cos\left[\gamma_K(\rho)\right] \Phi^{(-)}_{elec}\, |NJSKM_J\delta_{0\tau}\rangle + \sin\left[\gamma_K(\rho)\right]\, i\, \Phi^{(+)}_{elec}\, |NJSKM_J\tau\rangle$$

$$[17]\quad |b; NJSKM_J\tau\rangle = \cos\left[\gamma_K(\rho)\right]\, i\, \Phi^{(+)}_{elec}\, |NJSKM_J\tau\rangle - \sin\left[\gamma_K(\rho)\right] \Phi^{(-)}_{elec}\, |NJSKM_J\delta_{0\tau}\rangle$$

where $\Phi^{(-)}_{elec}$ is the electronic wavefunction for the lower Renner component $\tilde{X}\,^1A_1$, and $\Phi^{(+)}_{elec}$ is the electronic wavefunction for the upper component $\tilde{A}\,^1B_1$. In eqs. [16] and [17], $\delta_{0\tau}$ is a Kronecker Delta with $\delta_{00} = 1$ and $\delta_{01} = 0$. The angle $\gamma_K(\rho)$ determines, in a first approximation, the Renner interaction between these two electronic states. It is discussed in detail in section 15.4.2 of ref. 31. The rotation-spin basis functions $|NJSKM_J\tau\rangle$ (see refs. 25, 31) are symmetrized, simultaneous eigenfunctions of $\widehat{\mathbf{N}}^2$ [with eigenvalue $\hbar^2N(N+1)$], $\widehat{\mathbf{J}}^2$ [with eigenvalue $\hbar^2J(J+1)$], $\widehat{\mathbf{S}}^2$ [with eigenvalue $\hbar^2S(S+1)$], and $\widehat{J}_Z$, the component of $\mathbf{J}$ along the space-fixed quantization axis Z [with eigenvalue $\hbar M_J$] (see refs. 25, 31). Here, $\widehat{\mathbf{N}}$ is the total angular momentum of the molecule excluding spin, $\widehat{\mathbf{S}}$ is the electron spin, and $\widehat{\mathbf{J}} = \widehat{\mathbf{N}} + \widehat{\mathbf{S}}$. We assume that no electronic state other than the $\tilde{X}\,^1A_1$ – $\tilde{A}\,^1B_1$ pair of states contributes significantly to $\psi^{(i,J,M_J,S,\Gamma_{evr};\tau)}_{evr-ns}$. As indicated in eq. [15], the internal wavefunctions are labeled by the good quantum numbers J, M_J, S, and by Γ_{evr}, the irreducible representation spanned by $\psi^{(i,J,M_J,S,\Gamma_{evr};\tau)}_{evr-ns}$ in the molecular symmetry group C_{2v}(M) (1). The running index i numbers states with the same values of the good quantum numbers. This i is not to be confused with the i in Table 4. The parity of $\psi^{(i,J,M_J,S,\Gamma_{evr};\tau)}_{evr-ns}$ is $(-1)^\tau$, and $\tau = 0$ or 1. Φ_{ns} is an appropriate nuclear spin function.

The rovibronic wavefunctions given in eq. [15] are mathematically complicated, but they contain all accessible information about each rovibronic state. To obtain insight into the nature of the eigenfunctions, we have previously introduced and calculated the overall bending probability density function $f(\rho)$ of the states (32, 33). The quantity $dp = f(\rho)\,d\rho$ is the differential probability of finding the molecule with its bending angle between ρ and $\rho + d\rho$. For the ith state $\psi^{(i,J,M_J,S,\Gamma_{evr};\tau)}_{evr-ns}$, having energy E_i, the normalized probability density function for the bending angle $f_i(\rho)$ is given by

$$[18]\quad f_i(\rho) = \int_0^\infty dr_{12} \int_0^\infty dr_{32} \int_{rot,e,es,ns} dV\, |\psi^{(i,J,M_J,S,\Gamma_{evr};\tau)}_{evr-ns}|^2 = \sum_{\eta=a,b} \sum_{N=|J-S|}^{J+S} \sum_{K=0}^{N} \sum_{v_2^{(\eta)},v_2^{(\eta)'},N_{vib}^{(\eta)},\Gamma_{vib}^{(\eta)}} \left(c^{(i,J,M_J,S,\Gamma_{evr},\tau)}_{\eta,N,K,v_2^{(\eta)},N_{vib}^{(\eta)},\Gamma_{vib}^{(\eta)}}\right)^* \times c^{(i,J,M_J,S,\Gamma_{evr},\tau)}_{\eta,N,K,v_2^{(\eta)'},N_{vib}^{(\eta)},\Gamma_{vib}^{(\eta)}} \left(\Phi_{v_2^{(\eta)},K}(\rho)\right)^* \Phi_{v_2^{(\eta)'},K}(\rho)$$

where dV is the volume element associated with integration over the coordinates describing rotation, electronic orbital motion, electron spin, and nuclear spin.

In Fig. 1 we plot the bending probability distributions $f(\rho)$ for the the rotational level $J_{K_aK_c} = 1_{10}$ of the 12 members of the P = 10 polyad of the $\tilde{X}\,^1A_1$ state. In the following we shall be discussing emission transitions to these levels from the $J_{K_aK_c} = 0_{00}$ rotational level of the $7\nu_2$ state of $\tilde{A}\,^1B_1$ SiH_2; we plot the probability distribution of this level in Fig. 2.

A problem for $\tilde{X}\,^1A_1$ SiH_2 has been the assignment of the ν_1 and $2\nu_2$ states; these two states are in a strong Fermi resonance. The two $J = 0$ states of A_1 symmetry are observed at 1978.153 and 2005.469 cm^{-1}, respectively (12). Whereas Ishikawa and Kajimoto (10) initially assigned the highest level as $2\nu_2$ and the lowest level as ν_1, Hirota and Ishikawa (12) reversed these assignments. The wavefunction for the state at lower wavenumber has a 51.5% contribution from the $2\nu_2$ basis state and a 47.8% contribution from the ν_1 basis state. The state at higher wavenumber has a 51.7% contribution from ν_1 and a 46.7% contribution from $2\nu_2$. Consequently, as in ref. 12, we assign the lower state as $2\nu_2$ and the upper one as ν_1. The heavy mixing between the two states is also apparent in the probability distributions given in Fig. 3.

8. Simulation of spectra

To simulate spectra we use line positions obtained by calculating appropriate energy level differences, and intensities obtained from line strengths that are calculated from the square of the transition moment matrix elements involving the wavefunctions and ab initio transition moment surfaces given in eqs. [9]–[13]. The details of such a calculation are given in ref. 29. In Fig. 4 we show the result of simulating the emission spectrum from the 0_{00} rotational level of the $\tilde{A}$ (0,7,0) vibronic state to the 1_{10} levels of the $P = 10$ polyad of the $\tilde{X}$ state. For comparison we also show in this figure the observed spectrum from ref. 15[3] The relative intensities are extraordinarily sensitive to small changes in the potential energy functions and the agreement with experiment is not perfect; we underestimate the intensity of the transitions to the $i = 3$, 9, and 11 components. However, the weakness of the $i = 7$ and 10 components is correctly accounted for. The intensity distributions in our simulations of the emission spectra involving the other polyads are in broad agreement with the results in ref. 15, and all lines that could not be found experimentally are calculated as having low intensity relative to the observed lines. The strong transitions are generally those to states with high excitation of the bending mode. In such states, we get the highest vibronic transition moments with the initial state ($\tilde{A}\,^1B_1$ (0,7,0)), whose bending angle probability distribution is given in Fig. 2.

Initially in our fitting there seemed to be an interesting ambiguity in the assignment of the lowest two members ($i = 10$ and 11) of the polyad $P = 10$. In ref. 15 a level at 9306.07 cm^{-1} is observed and it is assigned as the i = 11 component of the P = 10 polyad; no level is assigned as the $i = 10$ component. Using the ab initio potential energy surfaces we find (see under the column headed "MCI Calc" in Table 4) that the $i = 10$ and 11 components of the $P = 10$ polyad are calculated at 9326.83 and 9151.24 cm^{-1}. Just looking at this result one would assign the 9306.07 observed term value as the $i = 10$ level rather than as the $i = 11$ level. However, the (obs–calc) deviations are large and negative for the lowest components of each polyad, and the assignment of the 9306.07 cm^{-1} level as $i = 11$, as done in ref. 15, is not unreasonable. Using this assignment we made the fitting to obtain the fitted potentials quoted here, and the simulation given in Fig. 4. We did try another fitting done just as above but with the single change of assigning the level at 9306.07 cm^{-1} as $i = 10$ in $P = 10$; the result for the $P = 10$ polyad is given in the column headed "Alternative" in Table 11, and the simulated $P = 10$ emission spectrum obtained using the alternative parameters is compared with the experimental spectrum[3] in Fig. 5. The relative intensities in the calculated spectrum using the alternative parameters are in very poor agreement with experiment, so although the fitting to the term values with the assignment of the 9306.07 cm^{-1} term value as $i = 10$ does not lead to unreasonable calculated term values it does lead to unreasonable calculated intensities. However, it is quite remarkable and alarming to us that with so much vibrational data there is still enough flexibility that it is possible to adjust the potential in a way that allows an alternative fitting to the same term value data but with a single level reassigned to have a substantial shift of about 100 cm^{-1}. We await with interest the results of further experiments to find more vibrational term values for singlet silylene.

[3] Reprinted from H. Ishikawa, Y. Muramoto, and N. Mikami. J. Mol. Spectrosc. **216**, 90 (2002). Copyright (2002) with permission from Elsevier.

Acknowledgments

We are very grateful to Professor Haruki Ishikawa for communicating his results to us before publication, and for some helpful correspondence. This work was initiated and supported under the auspices of a collaborative agreement between the National Research Council of Canada (NRC) and the National Science Council of Taiwan. The work of PJ was supported by the Deutsche Forschungsgemeinschaft and the Fonds der Chemischen Industrie. PJ is grateful to the Steacie Institute for Molecular Sciences for their hospitality.

References

1. P.R. Bunker and P. Jensen. Molecular symmetry and spectroscopy. 2nd ed. NRC Research Press, Ottawa, Ontario, Canada. 1998. See http://www.nrc.ca/cgi-bin/cisti/journals/rp/rp2_book_e?mlist1_90
2. P. Jensen and P.R. Bunker (*Editors*). Computational molecular spectroscopy. Wiley, Chichester, UK. 2000. See http://www.chem.uni-wuppertal.de/cms/
3. I. Dubois, G. Herzberg, and R.D. Verma. J. Chem. Phys. **47**, 4262 (1967).
4. I. Dubois. Can. J. Phys. **46**, 2485 (1968).
5. I. Dubois, G. Duxbury, and R.N. Dixon. J. Chem. Soc. Faraday Trans. 2, **71**, 799 (1975).
6. J.S. Francisco, R. Barnes, and J.W. Thoman. J. Chem. Phys. **88**, 2334 (1988).
7. R. Escribano and A. Campargue. J. Chem. Phys. **108**, 6249 (1998).
8. H. Ishikawa and O. Kajimoto. J. Mol. Spectrosc. **160**, 1 (1993).

9. C. Yamada, H. Kanamori, and E. Hirota. J. Chem. Phys. **91**, 4582 (1989).
10. H. Ishikawa and O. Kajimoto. J. Mol. Spectrosc. **150**, 610 (1991).
11. H. Ishikawa and O. Kajimoto. J. Mol. Spectrosc. **174**, 270 (1995).
12. E. Hirota and H. Ishikawa. J. Chem. Phys. **110**, 4254 (1999).
13. M. Fukushima, S. Mayama, and K. Obi. J. Chem. Phys. **96**, 44 (1992).
14. M. Fukushima and K. Obi. J. Chem. Phys. **100**, 6221 (1994)
15. H. Ishikawa, Y. Muramoto, and N. Mikami. J. Mol. Spectrosc. **216**, 90 (2002).
16. W. Gabriel, P. Rosmus, K. Yamashita, K. Morokuma, and P. Palmieri. Chem. Phys. **174**, 45 (1993).
17. W. Meyer. J. Chem. Phys. **58**, 1017 (1973).
18. G. Duxbury, A. Alijah, and R.R. Trieling. J. Chem. Phys. **98**, 811 (1993).
19. K. Andersson, M. Barysz, A. Bernhardsson, M.R.A. Blomberg, Y. Carissan, D.L. Cooper, T. Fleig, M.P. Fülscher, L. Gagliardi, C. de Graaf, B.A. Hess, G. Karlström, R. Lindh, P.-Å. Malmqvist, T. Nakajima, P. Neogrády, J. Olsen, B.O. Roos, B. Schimmelpfennig, M. Schütz, L. Seijo, L. Serrano-Andrés, P.E.M. Siegbahn, J. Stalring, T. Thorsteinsson, V. Veryazow, M. Wierzbowska, and P.-O. Widmark. MOLCAS. Version 5.2 [computer program]. Lund University, Sweden. 2001.
20. W.D. Allen and H.F. Schaefer. Chem. Phys. **108**, 243 (1986).
21. C.W. Bauschlicher, S.R. Langhoff, and P.R. Taylor. J. Chem. Phys. **87**, 387 (1987).
22. J. Berkowitz, J.P. Greene, H. Cho, and B. Ruščić, J. Chem. Phys. **86**, 1235 (1987).
23. J.W. Thoman, J.I. Steinfeld, R.I. McKay, and A.E.W. Knight. J. Chem. Phys. **86**, 5909 (1987).
24. P.-Å. Malmqvist and B.O. Roos. Chem. Phys. Lett. **155**, 189 (1989).
25. P. Jensen, M. Brumm, W.P. Kraemer, and P.R. Bunker. J. Mol. Spectrosc. **171**, 31 (1995).
26. M. Kolbuszewski, P.R. Bunker, W.P. Kraemer, G. Osmann, and P. Jensen, Mol. Phys. **88**, 105 (1996).
27. W.P. Kraemer, P. Jensen, and P.R. Bunker. Can. J. Phys. **72**, 871 (1994).
28. P. Jensen. J. Mol. Spectrosc. **132**, 429 (1988).
29. G. Osmann, P.R. Bunker, P. Jensen, and W.P. Kraemer. Chem. Phys. **225**, 33 (1997).
30. S.N. Yurchenko, M. Carvajal, P. Jensen, F. Herregodts, and T.R. Huet. Chem. Phys. **290**, 59 (2003).
31. P. Jensen, G. Osmann, and P.R. Bunker. *In* Computational molecular spectroscopy. *Edited by* P. Jensen and P.R. Bunker. Wiley, Chichester, UK. 2000.
32. G. Osmann, P.R. Bunker, W.P. Kraemer, and P. Jensen. Chem. Phys. Letters **309**, 299 (1999).
33. G. Osmann, P.R. Bunker, W.P. Kraemer, and P. Jensen. Chem. Phys. Lett. **318**, 597 (2000).

This article has been cited by:

1. Yanan Wu, Chunfang Zhang, Haitao Ma. 2017. Ab initio conical intersections for the Si(1 D) + H 2 reaction system: a lowest five singlet states study. *RSC Advances* **7**:20, 12074-12084. [Crossref]
2. Damian L. Kokkin, Tongmei Ma, Timothy Steimle, Trevor J. Sears. 2016. Detection and characterization of singly deuterated silylene, SiHD, via optical spectroscopy. *The Journal of Chemical Physics* **144**:24, 244304. [Crossref]
3. David E. Woon, Eric Herbst. 2009. QUANTUM CHEMICAL PREDICTIONS OF THE PROPERTIES OF KNOWN AND POSTULATED NEUTRAL INTERSTELLAR MOLECULES. *The Astrophysical Journal Supplement Series* **185**:2, 273-288. [Crossref]
4. S. N. Yurchenko, B. A. Voronin, R. N. Tolchenov, N. Doss, O. V. Naumenko, W. Thiel, Jonathan Tennyson. 2008. Potential energy surface of HDO up to 25000cm−1. *The Journal of Chemical Physics* **128**:4, 044312. [Crossref]
5. R. Guérout, P. R. Bunker, Per Jensen, W. P. Kraemer. 2005. A calculation of the rovibronic energies and spectrum of the BA11 electronic state of SiH2. *The Journal of Chemical Physics* **123**:24, 244312. [Crossref]
6. Yasuhiko Muramoto, Haruki Ishikawa, Naohiko Mikami. 2005. First observation of the BA11 state of SiH2 and SiD2 radicals by optical-optical double resonance spectroscopy. *The Journal of Chemical Physics* **122**:15, 154302. [Crossref]